A Novel Hybrid Feedstock to Liquids and Electricity Process: Process Modeling and Exergoeconomic Life Cycle Optimization

Chang He
State Key Laboratory of Heavy Oil Processing, College of Chemical Engineering, China University of Petroleum, Beijing 102249

Fengqi You
Dept. of Chemical and Biological Engineering, Northwestern University, Evanston, IL 60208

Xiao Feng
State Key Laboratory of Heavy Oil Processing, Inst. of New Energy, China University of Petroleum, Beijing 102249

DOI 10.1002/aic.14551
Published online July 18, 2014 in Wiley Online Library (wileyonlinelibrary.com)

This article proposes a novel hybrid low-rank coal (LRC)/biomass/natural gas process for producing liquid fuels and electricity. The hybrid process highlights coexistence of indirect and direct liquefaction technologies, cogasification of char and biomass, and corefinery of LRC syncrude and Fischer–Tropsch syncrude. A process simulation based on detailed chemical kinetics is present to illustrate its feasibility. In addition, we propose an exergoeconomic life cycle optimization framework that seeks to maximize the primary exergy saving ratio, primary total overnight cost saving ratio, life cycle waste emissions avoidance ratio, and primary levelized cost saving ratio by comparing the proposed hybrid process to its reference stand-alone subsystems. From the results, we can determine four optimal designs which yield competitive breakeven oil prices ranging from \$1.87/GGE to \$2.13/GGE. © 2014 American Institute of Chemical Engineers *AIChE J*, 60: 3739–3753, 2014

Keywords: low-rank coal, hybrid process, process simulation, life cycle optimization

Introduction

Low-rank coals

Substantial effort around the world is currently directed toward achieving greater energy independence through the utilization of a more diverse array of primary energy sources. Of particular interest are liquid fuels that can be derived from nonpetroleum-based fuels, namely coal, natural gas, and biomass.[1] Among these alternative fuels, high/moderate-rank coals (HRCs, e.g., anthracite and bituminous) are the most investigated fuels due to their low prices and rich geological storage. However, half of the world's coal reserves are low-rank coals (LRCs) such as sub-bituminous and lignite. Compared to HRCs, the LRCs contain high inherent moisture, volatiles, and ash, which significantly reduce their heating values. This drawback hinders the commercial application of coal to liquid fuels (CTL) technology, which is further constrained when high levels of impurities like oxygen, sulfur, and alkali metals are present in LRCs. Conversely, most LRCs are reported to be rich in volatiles and organic liquids, which in general command a substantially higher price than syngas. Typical engineering analysis[2] shows that the energy density (GJ/ton) and economic value (\$/ton) shares of the extractable liquids in LRCs are about 68% and 75%, respectively, although they account for only 11.5 wt % of LRCs.

Decoupling gasification techniques

Decoupling gasification (DCG) techniques are used to decouple the complicated reaction networks in a gasification process by isolating, inhibiting, or enhancing one or some subreactions (pyrolysis, cracking, reforming, gasification, and combustion), thus reorganizing the targeted subreactions.[3] DCG techniques have been implemented in various thermal conversion processes, including dual-bed gasification[4] and chemical looping gasification,[5] and so forth. In this way, we can separate the pyrolysis subreaction and enhance the extraction of liquid products from LRCs using direct liquefaction pathway. The extracted liquid products can be further upgraded in a refinery plant, while the remaining product, mainly LRC char (a kind of upgraded coal, 80–95 wt %), is not only a value-added metallurgical fuel but also a high-quality raw material suitable for building a syngas-based multiproduction platform.

Hybrid feedstock processes and structures

When LRC char is used as the carbon resource, issues such as environmental impact and economic performance

Additional Supporting Information may be found in the online version of this article.

Correspondence concerning this article should be addressed to Xiao Feng at xfeng@cup.edu.cn.

must be addressed. Liquid fuels generated from char/coal without CO_2 capture and storage (CCS) will result in net greenhouse gas (GHG) emissions that are about two times those from petroleum fuels.[6] Even with the CCS option, the life cycle GHG emissions of a CTL plant are still about 25% higher than those of a petroleum refinery.[7] One effective approach to reducing life cycle GHG emissions involves the use of hybrid energy processes that combine the utilization of multifeedstock and the coproduction of alternative fuels and power. Compared to traditional standalone processes, recent studies have shown that hybrid processes can present more opportunities to achieve less environmental footprint in a cost-effective way.[8,9] These systems can be classified into two categories: (1) Multifeed input structure: the generation of intermediates like syngas is the first step that generally includes two complementary ways for inputs. One way features "material + fuel,"[10] which is a primary approach for saving expensive fuels. The other way is "material + material,"[11,12] which is the more advanced form that includes separate gasification and cogasification operations; (2) Multiproduct output structure: there are three types of structure, namely parallel,[13,14] sequential,[15] and mixed structures.[16] The parallel structure offers greater operational flexibility by adjusting the syngas distribution. The sequential structure maximizes the chemical energy conversion rate, in which the syngas passes the once-through (OT) chemical synthesis unit without recycle. The mixed structure is a combination of the first two structures, giving the benefits of both structures.

This article presents a novel hybrid process, designated here as LRC/biomass/natural gas to liquids and electricity process (l-CBGTL). Two basic process configurations, RC and OT, are considered within this process. A detailed process simulation is performed with the Aspen Plus v7.3 package to illustrate its technoeconomic feasibility. Finally, we develop an exergoeconomic life cycle optimization framework and propose several useful indicators that can be used to quickly assess and optimize the process performance from the energetic, economic, and environmental perspectives. These indicators are termed as primary exergy saving ratio (PES), primary total overnight cost saving ratio (POS), life cycle waste emissions avoidance ratio (EmA), and primary levelized cost saving ratio (LCS). In this way, the optimum process design, key operating parameters, and production scales can be simultaneously determined on the basis of the same amount of products. The novelties of this article include: (1) The first innovative process design that integrates indirect and direct liquefaction technologies and considers the corefinery of the corresponding liquid products (FT and LRC syncrudes); (2) The first nonlinear programming (NLP) model for rigorous estimation of the complex distribution of LRC pyrolysis products; and (3) A systematic optimization approach for hybrid energy systems that is capable of generating multiobjective designs.

Conceptual Design and Plant Configuration

Figure 1 shows the proposed l-CBGTL process design, which mainly includes eight process units, namely LRC pyrolysis, biomass and char cogasification, air separation, crude syngas treatment, natural gas reforming and hydrogen production, FT synthesis, power plant, and hydrocarbons upgrading. In this figure, the pretreated LRC first enters the pyrolyzer where the vapor-phase products and char are generated. The vapor-phase products pass through the cyclone and filter to sequentially remove ash and small particles. The LRC syncrude and pyrolysis gas are recovered from the purified products via the oil recovery. The product char from the pyrolyzer bottom is mixed with dry biomass to be cogasified to produce crude syngas. In the syngas treatment unit, the crude syngas together with the pyrolysis gas are cleaned up and most of the acid gases are taken out. Another source of syngas produced from natural gas reforming is divided into two streams. One stream is used as the H_2-rich syngas to raise the H_2 content of biomass/char-derived syngas while the other stream is used to generate high quality refinery H_2.

In the FT synthesis unit, large amounts of unreacted gases are separated from the raw FT effluent, which mainly include unconverted syngas and light ends ($C_1 \sim C_4$) generated from FT synthesis. Depending on whether or not this stream is finally recycled to the FT reactor, the following two basic configurations may be envisaged. (1) Unreacted gases recycle (RC) configuration (see Fig. 1a): the clean syngas from the syngas treatment unit is split into two streams. One stream is sent to the combined cycle for power generation and the other one is used as raw material for FT synthesis. Note that about 3% of unreacted gases is sent to the gas turbine (GT) furnace to prevent inert gas accumulation; (2) OT configuration (see Fig. 1b): the clean syngas is mixed with natural gas-derived syngas and then passes through the FT reactor only once. All unreacted gases plus light ends from hydrocarbon upgrading are compressed and supplied to the power plant. After FT synthesis, both FT and LRC syncrudes are upgraded to final liquids.

Two precombustion carbon mitigation alternatives are considered in this design, which are located in front of the combined cycle and pressure swing adsorption (PSA). The carbon mitigation design consists of two steps. First, 98% of CO is shifted to H_2 via the water gas shift (WGS, see Eq. 5) reaction, and then, the H_2-rich stream runs through the CO_2 capture section where the lean methanol (MeOH) is used as the absorbent to remove around 95% of CO_2 in the syngas. Besides, in the RC configuration the H_2-rich syngas needs a CO_2 capture section to remove CO_2 to avoid accumulation of recycled CO_2.

Feedstock properties of LRC and biomass are given in Tables S-1 and S-8 of Supporting Information (SI) I, and the composition of natural gas is given in Table S-9 of SI I.

Process Modeling

LRC pyrolysis

$$\begin{aligned} &C_aH_bO_cN_dS_d(H_2O)_wA(\mathrm{LRC}) + \mathrm{Steam} + \mathrm{FeO/Fe_2O_3(O_2\text{-}carrier)} \xrightarrow{\text{cat.}} CO + H_2 \\ &\quad + CO_2 + SO_2 + CH_4 + H_2S + NH_3 + N_2(\text{pyrolysis gas}) + C_\alpha H_\beta O_\gamma N_\delta S_\varepsilon A(\text{char}) \\ &+ C_jH_\phi O_\chi(\text{LRC tar}) + wH_2O\ (\text{water}) + Fe \end{aligned} \tag{1}$$

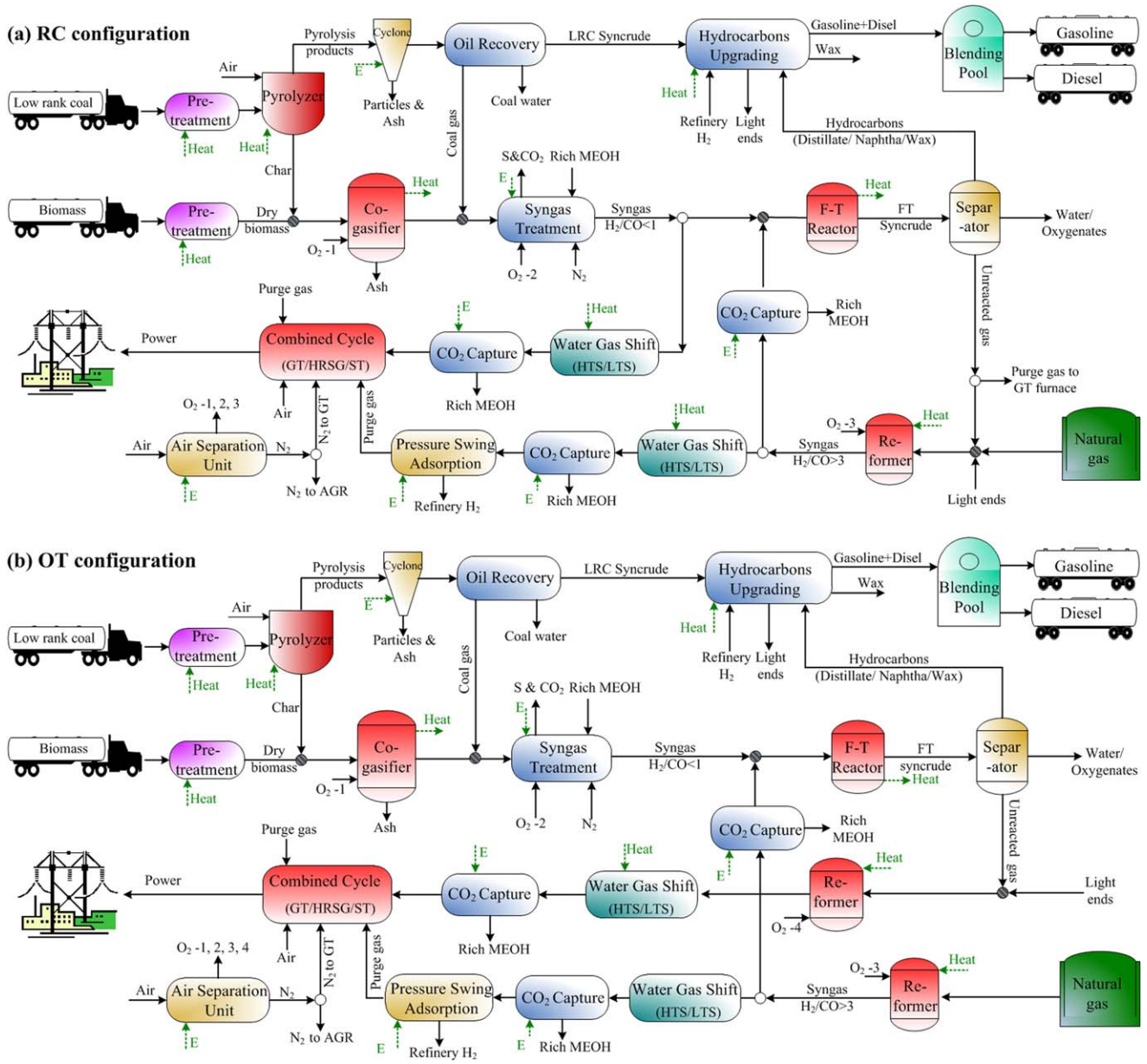

Figure 1. Proposed I-CBGTL process design.

(a) RC configuration; (b) OT configuration. [Color figure can be viewed in the online issue, which is available at wileyonlinelibrary.com.]

$$C_\eta H_\phi O_\chi(\text{LRC tar}) + H_2 \xrightarrow{\text{cat.}} C_\eta H_\phi O_\chi \ (\text{LRC syncrude}) \quad (2)$$

The low/moderate temperature pyrolysis process considered here is based on a literature report.[17] In the pretreatment process, the raw LRC is crushed and ground into particles with diameter between 10 and 50 mm, and dried to below 12 wt % moisture content. Then, the dry LRC enters a fixed-bed pyrolyzer where it is thermochemically decomposed into complex products (char, tar, pyrolysis gas, etc., see Eq. 1) by reacting with moderate pressure steam ($m_{\text{MPsteam}}/m_{\text{dafLRC}} = 0.45$) and iron-based catalytic O_2-carrier ($m_{\text{FeO}}/m_{\text{dafLRC}} = 0.14$, $m_{\text{Fe}_2\text{O}_3}/m_{\text{dafLRC}} = 0.12$). But the LRC tar has a low H/C ratio and high poly-nuclear aromatic content, which can be further hydro-reacted with highly reactive H_2 in the pyrolysis gas by adding FeS_x catalysts and ultimately upgraded to LRC syncrude (Eq. 2). Based on experimental data,[17] we formulate an NLP model that accounts for mass/atomic balances to determine the actual yields, covering 29 components in LRC syncrude, nine components in pyrolysis gas, seven components in char, and four other by-products (Fe, ash, etc.). The generic optimization problem of this NLP model minimizes the sum of the difference between the calculated yields (N_j or m_i) and experimental data (N_j^* or m_j^*), under the given operating conditions and LRC type. Detailed information on product j and constraints are given in SI I. The model formulation is present blow.

$$\text{Find}: N_i \text{ or } m_i$$

$$\text{Minimize}: \lambda = \sum_{j=0}^{i} \left(\psi_j \times S_{\text{ratio},j}\right) j < i$$

$S_{\text{ratio},j} \le \left|N_j/N_{j+1} - N_j^*/N_{j+1}^*\right|$ and $S_{\text{ratio},j} \le \left|\sum N_j/\sum N_{j+1} - \sum N_j^*/\sum N_{j+1}^*\right|$; within the constraints of atomic balance (at), mass balance (ma), and compositional limitation

$$\text{at}(a, sp) = 0; \text{ma}(a, sp) = 0$$

$$N_{i,\text{lo}}^* \le N_j \le N_{j,\text{u}}^*; m_{j,\text{lo}}^* \le m_j \le m_{j,\text{u}}^*; S_{\text{ratio}} \ge 0; N_j \ge 0$$

where S_{ratio} is the specific relationship between certain species; ψ is the relative importance of the coefficient S_{ratio}; a and sp are atoms and species involved in the LRC pyrolysis process; the subscripts lo and u are the lower and upper bounds. The pyrolysis process model is optimized in the GAMS 22.3 modeling system. Solving this model to identify its global optimality using the global solver BARON[18] gives the N_i values listed in Table S-7 of SI I.

In this work, the LRC pyrolyzer is modeled using the RYield module in the Aspen Plus library that integrates an external FORTRAN subroutine using data listed in Table S-7 of SI I. The overall conversion rate of dry LRC and char loss rate are specified as 87% and 5%, respectively.[19] Furthermore, the LRC syncrude and pyrolysis gas are assumed to be perfectly recovered vapor-phase products via the oil recovery.

Biomass and char cogasification

Prior to cogasification, the biomass should be dried to less than 10 wt % moisture content in the pretreatment processes. The cogasifier examined in this study is a Shell-type dry-feed, O_2- blown, and entrained flow gasifier, to which the char and biomass are simultaneously cofed. High pressure (4.2 Mpa) and temperature (1200–1500°C) crude syngas is generated in the presence of 95 mol % O_2 and MP steam. Currently, gasification facilities using a dry-fed Shell gasifier have been designed for a cofeed of up to 30% biomass on an energy basis.[14,20] The gasifier is modeled using the RYield and RGibbs modules. Char and biomass are broken down into solids (C, S, and ash), and gases (H_2, O_2, Cl_2, and N_2) in the RYield module, while the cogasification reactions occur in the RGibbs module which calculates rigorous reactions and multiphase restricted-equilibrium based on Gibbs free energy minimization. The major reactions and temperature approaches shown in Eqs. 3–9 are specified to match the experimental and industrial data for the Shell gasifier.[21] The syngas leaving the gasifier contains mostly CO (50–66 mol %) and H_2 (20–30 mol %). CO_2, H_2S, and COS are present in lower molar quantities.

$$C + O_2 \rightarrow CO_2 \qquad 0^\circ C \qquad (3)$$

$$C + 0.5O \rightarrow CO \qquad 0^\circ C \qquad (4)$$

$$CO + H_2O \rightarrow CO_2 + H_2 \qquad -250^\circ C \qquad (5)$$

$$CH_4 + H_2O \rightarrow CO + 3H_2 \qquad -100^\circ C \qquad (6)$$

$$COS + H_2O \rightarrow CO_2 + H_2S \qquad 0^\circ C \qquad (7)$$

$$H_2 + S \rightarrow H_2S \qquad 0^\circ C \qquad (8)$$

$$N + 3H_2 \rightarrow 2NH_3 \qquad 0^\circ C \qquad (9)$$

It is assumed that 0.5% of the fixed carbon is unconverted and 4% of the HHV of the fuel is lost to the environment. Two heat exchangers in series are used to simulate the cooling section. First, the radiant heat is recovered in the heat recovery steam generation (HRSG) section with a specified temperature of 600°C. Slag (molten ash and unconverted carbon) is assumed to be solidified at this point and totally rejected via a slag filter. Then, slag-free syngas continues to be cooled down to 250°C in a waste heat boiler, in which the outlet stream is mixed with the pyrolysis gas with the mixture going to the sour water treatment section. In this section, a scrubber first removes 99% of chlorides from the mixture by adding weak alkaline water. The scrubber bottom stream is mixed with sour water form the Claus plant, and sent to the sour water stripper to strip CO_2, H_2S, and NH_3. The stripper overhead off-gas containing about 40 wt % (dry basis) H_2S is sent to the Claus plant for sulfur recovery. A detailed waste water treatment step is not considered in this work.

Crude syngas treatment

Acid Gas Removal (AGR) Section and CO_2 Compression Section. The AGR section removes acid impurities such as COS, CO_2, and H_2S. The crude syngas first passes through a COS hydrolyzer where 100% of the COS is converted to H_2S via the hydrolysis reaction (see Eq. 7).[22] After that, the syngas is cooled down to 40°C and fed to a Rectisol process. In this process, H_2S and CO_2 are sequentially absorbed in the H_2S absorber and CO_2 absorber by contacting with MeOH solvent at an MeOH:syngas molar ratio of about 0.5, and subsequently released by heating the solvent. The H_2S absorber captures most of the H_2S but CO_2 is partially removed because its solubility in MeOH solvent is significantly lower than that of H_2S. The rest of the CO_2 is captured in the CO_2 absorber where its full absorption is favored by the low temperature of MeOH solvent (−40°C). Next, the H_2S-rich MeOH from the bottom of the H_2S absorber and the tail gas stream from the Claus/Shell Claus Off-gas Treatment (SCOT) section are contacted with N_2 from the air separation unit (ASU; N_2/crude syngas molar ratio = 0.2) in the H_2S concentrator to strip the volatile compounds. The H_2S concentrator bottom stream is sent to the MeOH stripper which can deeply remove H_2S from the solvent. In this way, essentially all H_2S is rejected in the acid gas leaving only roughly 30 ppm H_2S in the purified syngas, while about 80% of CO_2 is captured by the solvent. The acid gas mixture (about 70 mol % H_2S and 25 mol % CO_2) exiting from the top of the MeOH stripper is routed to the Claus/SCOT section for producing elemental sulfur.

Both the RC and OT configurations are modeled with CCS option. The stripped MeOH solvent from the bottom of MeOH stripper is mixed with makeup MeOH solvent and then split into three branches. The first branch, accounting for 60–70% of the total, is chilled to −40°C and routed to the top of the CO_2 absorber. The remaining two branches are sent to the hydrogen production and power plant. A portion of the loaded solvent (20–30%) from the bottom of the CO_2 absorber is chilled to −25°C and sent to the H_2S absorber. The remaining portion of the loaded solvent, together with the lean MeOH solvent from other CO_2 capture sections, passes through HP, MP, and low pressure (LP) flash drums to flash off CO_2 at different decreasing pressures (20/10/1.5 atm). The low-pressure CO_2-rich vapor from the LP flash is compressed and recycled to the CO_2 absorber. Three intercooled stages are used for compressing the LP

CO_2-rich vapor to the pressure of MP CO_2-rich vapor. Thereafter, MP CO_2-rich vapor is cooled, dehydrated, and further compressed to 150 atm to be transported through pipelines to a sequestration site.

Claus/SCOT Section. The sulfur compounds (S_X) are recovered from the acid gas in an oxygen blown, multistep sulfur recovery section, which successively contains one thermal stage, two catalytic stages, and one SCOT stage. In the thermal stage, stoichiometric amount of oxygen generated in the ASU is added to oxidize 34.0% of the H_2S to SO_2 in the Claus furnace, producing a feeding gas with an H_2S/SO_2 molar ratio of 2 for the catalytic stages, while the off-gas formed in the cogasification unit is fed directly to here for destruction of NH_3. In the catalytic stages, the remaining H_2S is converted to S_X. The S_X are condensed and collected as a saleable by-product (97 mol % purity). The Claus tail gas contains small but varying amount of SO_2 compound (0.5–5.0 mol %), which needs to be essentially removed via a SCOT stage. In the SCOT stage, the Claus tail gas passes through a preheater to heat up to the reaction temperature (300°C) before entering a catalytic hydrogenation reactor, which converts 99.9% of SO_2 to H_2S ($3H_2+SO_2=H_2S+2H_2O$). The SCOT effluent is cooled first in a cooler to 160°C, and then condensed in a knockout drum to approximately 35°C. The sour water from the knockout drum goes to the sour water stripper (in biomass and char cogasification unit) for further degrading. Finally, the H_2S content (about 3 mol %) present in the overhead stream is compressed to 42 atm before being recycled to the AGR section.

Air separation

For the ASU, a cryogenic, integrated nitrogen injection ASU option is recommended due to its cost-saving benefit.[23] In this unit, the product nitrogen (99 mol %) is used in two ways. In the first way, nitrogen is compressed and sent to the AGR section to realize the targeted H_2S concentration and in the second way it is used as a diluent for the H_2-rich syngas fed to the GT furnace. The addition of N_2 diluent reduces the flame temperature and leads to additional power production in the turbine with lower NO_x emissions. The product O_2 is assumed to be 95 mol %, with 3.65 mol % Ar and 1.35 mol % N_2 mixed within it. Most of the O_2 is compressed to gasifier pressure and fed into the cogasifier, and the rest is sent to the autothermal reformer (ATR) reactor and the Claus furnace. The amount of air supplied to the ASU is determined by the amount of O_2 required by the gasifier and Claus plant. The total ASU power requirement (P_{ASU}) is based on the specified purity of O_2 which may be estimated according to the following correlation[21]

$$P_{ASU}=P_{aircomp}\times\beta$$
$$\beta=\begin{cases}5.4992\times C_{O_2}, & C_{O_2}\in(95\%,97.5\%)\\ 8.295\times10^2/(100-C_{O_2}{}^{1.136})+0.988618, & C_{O_2}\in(97\%,99.5\%)\end{cases} \quad (10)$$

where $P_{aircomp}$ is the net power consumption of the main air compressor (MWh); C_{O2} is the O_2 molecular purity (mol %).

Natural gas reforming and hydrogen production

For the natural gas reforming section, the fresh natural gas (see Table S-9 in SI I) mixed with light ends and unreacted gases (only existing in the RC configuration), is converted to H_2-rich syngas. The mixture (roughly 98 mol % CH_4) first passes through the prereformer and ATR. The prereformer is used to avoid heavy hydrocarbons cracking in the next ATR reactor, and the reactions taking place here are given by Eq. 11 where all species heavier than CH_4 are converted into syngas. Additionally, the side reactions described by Eqs. 5 and 12 approach equilibrium

$$C_nH_m+2H_2O\rightarrow(n+0.5m)H_2+nCO \quad (11)$$
$$CO+3H_2O\leftrightarrow CH_4+H_2O \quad (12)$$

The ATR reduces CH_4 in the stream to syngas by reacting the CH4 with MP steam (Steam/C molar ratio = 0.6) and oxygen (O_2/C molar ratio = 0.65) supplied by the ASU. It is modeled as an adiabatic equilibrium reactor according to Eqs. 5, 6, and 13, resulting in that the ATR outlet contains about 65 mol % H_2, 25 mol % CO, and 7 mol % CO_2. The ATR outlet then splits into two branches: (1) One branch, accounting for 90–95% of total H_2-rich syngas, is directly routed to the FT synthesis unit; (2) The other branch goes to a hydrogen production section where high quality H_2 is generated for upgrading of LRC and FT syncrudes. The hydrogen production section comprises high-temperature-shift reactor (HTS, 300–450°C), low-temperature-shift reactor (LTS, 200–300°C), CO_2 absorber, and PSA. The WGS reaction occurs inside the HTS and LTS reactors which are connected in series; both are modeled as adiabatic plug flow reactor. The pertinent kinetic parameters are given in SI I

$$CH_4+1.5O_2\leftrightarrow CO+2H_2O \quad (13)$$

Both the ATR and WGS reactions are strong exothermic reaction, and the interstage coolers are used to cool down the outlet streams from the ATR and HTS reactors by raising a portion of the shift steam (350°C, 27 atm). The H_2-rich stream exiting the LTS reactor passes two coolers in series to cool down to ambient temperature for dehydrating before entering the CO_2 absorber. In the CO_2 absorber, about 90% of CO_2 in the feed is captured by the low-temperature rich MeOH solvent (−40°C) and the lean MeOH from the bottom of the CO_2 absorber is sent back to the AGR section. The PSA block is modeled as an "SSPLIT" separator on the basis that PSA recovery and purity are not sensitive to changes in the composition and pressure of the inlet stream. The PSA block is designed to recover 90 % of the H_2 in the inlet at 99.5 mol % purity, as shown below

$$MF_{H_2,out}=\frac{0.9mf_{H_2}\times MF_{H_2,in}}{0.995} \quad (14)$$
$$mf_{j,out}=(1-0.995)\frac{mf_{j,in}}{\sum mf_{j,in}}\ j=\{CO_2,CO,N_2,AR,CH_4\} \quad (15)$$

where $MF_{H_2,out}$ and $MF_{H_2,in}$ are the molar flow rate (kmol/hr) of H_2 and feed stream, respectively; $mf_{j,out}$ and $mf_{j,in}$ are,

Table 1. Composition of LTFT Syncrude and LRC Syncrude on a Mass Basis

Species Name	LTFT Syncrude[a]	LRC Syncrude[b]
Light ends	8.98	–
C_1	4.49	–
C_2–C_4 paraffins	0.9	–
C_2–C_4 olefins	3.59	–
Naphtha	26.86	29.94
C_5–C_{10} paraffins	6.88	10.90
C_5–C_{10} olefins	16.06	10.60
Aromatics	–	8.44
Distillate	38.12	54.70
C_{11}–C_{22} paraffins	26.91	21.65
C_{11}–C_{22} olefins	11.21	15.40
Aromatics	–	17.65
Wax	28.46	11.95
C_{23}–C_{29} paraffins	12.52	3.70
C_{23}–C_{29} olefins	–	–
C_{30+} heavy wax	15.94	4.22
Aromatics	–	4.03
Oxygenates	1.50	–
Vapor phase	0.10	–
Aqueous phase	1.00	–
Organic phase	0.40	–
N/S-compounds	–	3.43
API	40	45
Reid vapor	1.1	0.9
Centane/octane number	24/87	27/85
Average MW	97	115

[a]LTFT syncrude composition excludes inert gas (N_2) and WGS products (CO, CO_2, H_2O, and H_2).
[b]This LRC syncrude composition is summarized from Table S-7 of SI I.

respectively, the molar fraction of impurity species j in H_2 and feed stream. The purge gas leaving the PSA block is sent for combustion in the GT furnace.

FT synthesis

The CO-rich syngas ($H_2/CO \approx 0.4$) leaving the syngas treatment unit is mixed with the H_2-rich syngas ($H_2/CO \approx 3$) from the ATR reactor, and the resulting mixture exchanges heat with the vapor cooler before going to the FT synthesis reactor where a high exothermic FT reaction takes place. The FT synthesis reaction (Eq. 16) mainly converts syngas into a range of straight-chain hydrocarbons (syncrude) that can be refined into naphtha and distillate fractions, which can then be upgraded to diesel and gasoline in the hydrocarbons upgrading unit. In this work, we consider the operating conditions of low temperature (210°C, LTFT) and moderate pressure (3.0 MPa) which favor the production of distillate hydrocarbons and waxes

$$n\mathrm{CO}+(n\text{-}q+0.5m)\mathrm{H_2} \rightarrow \mathrm{C}_n\mathrm{H}_m\mathrm{O}_q+(n\text{-}q)\mathrm{H_2O} \quad (16)$$

$$\mathrm{C}_n\mathrm{H}_m\mathrm{O}_q \equiv \{\text{lightends}+\text{naphtha}+\text{distillate}+\text{wax}+\text{oxygenates}\} \quad (17)$$

where $C_nH_mO_q$ denotes the paraffin and olefin main products; n, m, and q denote the number of carbon, hydrogen, and oxygen atoms in the hydrocarbons, respectively. The hydrocarbon products $C_nH_mO_q$ can be lumped into five types of products, namely light ends, naphtha, distillate, wax, and oxygenates (see Eq. 17). Hydrocarbon products up to C_{29} are represented by paraffin and olefin compounds. Detailed information on these products is listed in Table 1. In addition to the LTFT synthesis reaction, the WGS reaction is unavoidable.[24] In this study, a slurry phase reactor with iron-based catalysts is preferred, which can promote contact efficiency and compensate for suboptimal syngas composition.[15] The LTFT synthesis kinetic reactions and products are given in SI I. The syngas composition is a key factor that should satisfy the stoichiometry of H_2/CO molar ratio. For the Shell-type gasifier and LTFT synthesis, it is recommended that the H_2/CO ratio should fall within 0.67–2.00.[25–28]

Power plant

The power plant includes the CO_2 capture, GT, steam turbine (ST), and HRSG sections. The CO_2 capture section, including an HTS reactor and a CO_2 absorber, reduces the CO to below 8% in the syngas and captures about 80% of CO_2 before the syngas combustion. The GT generates power by converting the chemical energy in the H_2-rich syngas and combustible waste streams into shaft work. The GT section includes a syngas saturator/expander, an air compressor, a GT furnace, and a GT. A certain amount of pressurized N_2 from the ASU is injected to dilute the H_2-rich syngas to lower the low heating value (LHV) of syngas fuel to 4.30 MJ/Nm^3 as well as reduce the NO_x formation.[21] The flue gas from the GT section exchanges heat with process steam streams in the HRSG to provide the steam needed in the steam turbines which also produce work. The HRSG section in this model has three pressure levels: HP; 12.4 MPa and 540°C, MP; 4.0 MPa and 540°C and LP; 1.24 MPa and 370°C. The work produced from the GT and ST is converted to electricity through electricity generators.

Hydrocarbons upgrading

Table 1 shows the hydrocarbon products fractions of LTFT synthesis (210°C and $H_2/CO = 1$) and LRC pyrolysis. LTFT syncrude is characterized by a carbon number distribution that is rather heavy and it contains essentially no aromatics, N-compounds, or S-compounds. In LTFT syncrude, the hydrocarbon products up to C_{29} are represented by paraffins and olefins, where the empirical fraction of carbon in the paraffin form is 50% for C_2, 23% for C_3–C_4, 30% for C_5–C_{10}, 70% for C_{11}–C_{22}, and 99.9% for C_{23}–C_{29}.[29,30] Besides, C_4–C_6 have both linear and branched forms with a linear carbon fraction of 95% for C_4, and 90% for C_5 and C_6.[27,28] Wax refers to hydrocarbons with carbon numbers more than 22. All C_{30+} species are represented by a generic wax pseudocomponent $C_{52.524}H_{105.648}O_{0.335}$.[27,28] Oxygenate species formed in the LTFT reactor are represented by vapor phase ($C_{2.43}H_{5.69}O$), aqueous phase ($C_{1.95}H_{5.77}O_{1.02}$), and organic phase ($C_{4.78}H_{11.14}O_{1.1}$) pseudocomponents, where the total carbon conversion rate for each species is 0.1%, 1.0%, and 0.4%, respectively.[27,28] Comparing to LTFT syncrude, LRC syncrude contains more distillate and aromatics while small amounts of N and S compounds are present.

In this article, the proposed corefinery design follows a detailed model developed by Liu et al.[31] which can produce gasoline and diesel blendstocks that meet the EU-4 standards. As shown in Figure S-8 in SI I, the LTFT and LRC syncrudes are first sent to a hydrocarbons recovery unit where they are separated into naphtha, distillate, and wax. The three intermediates enter the naphtha hydrotreater, distillate hydrotreater, and wax hydrocracker, respectively. Hereafter, The C_5/C_6 paraffin separated from the hydrotreated naphtha goes to the C_5/C_6 isomerizer which converts n-paraffin to i-paraffin to improve the octane value, and the remaining C_{6+} naphtha is sent to the Pt-zeolite reformer

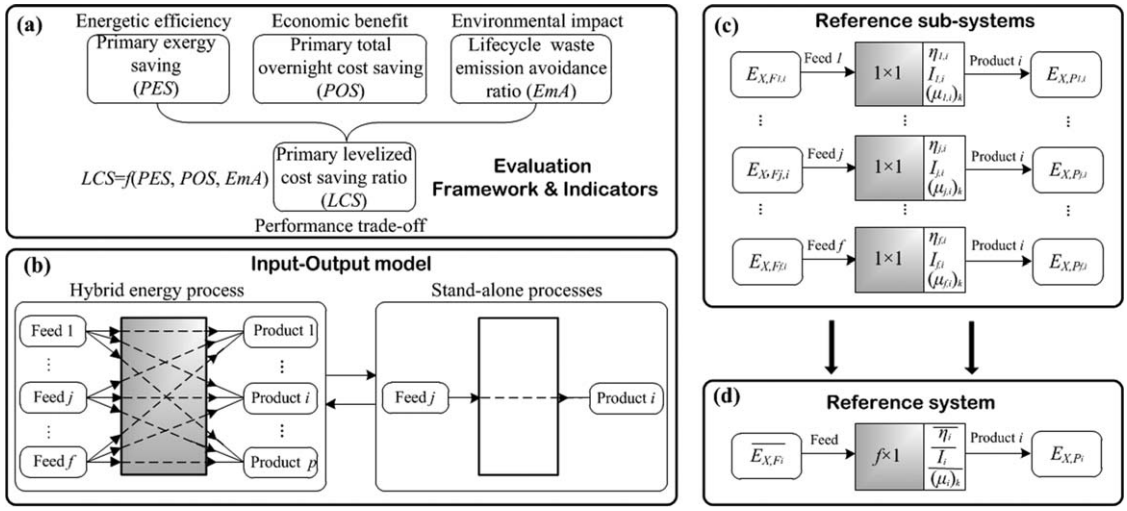

Figure 2. Optimization framework and indicators for hybrid energy systems.

which converts all cycloalkanes and around 60% of *n*-paraffin to reformates and H_2. The hydrotreated distillate with low octane value is sent to the diesel pool as the diesel blendstock. Furthermore, the hydrocracked wax is split into four streams as follows: (1) the light ends (C_2–C_4) together with light ends generated from other reactors are sent to the natural gas reforming section as feedstocks; (2) C_5/C_6 paraffins enter the C_5/C_6 isomerizer; (3) the stream containing $C_{13} \sim C_{20}$ hydrocarbons is used as diesel blendstock; (4) the remaining hydrocarbons enter the ZSM-5 reactor in which 60–80% of *n*-paraffin is converted to *i*-paraffin via the non-H_2 upgrading technologies. Each reactor shown in Figure S-8 of SI I is modeled using the RSTIC module and the corresponding reactions are given in Table S-11 of SI.

Process simulation and modeling parameters

The Aspen Plus model, consisting of chemical reactions and unit operations, thermodynamic property methods and stream class selection, and process simulation and synthesis, is built based on open literature reports and expert interviews. Detailed process description and key operating parameters of the proposed l-CBGTL process are given in SI I.

Exergoeconomic life cycle optimization framework

Relative saving indicator has a long history of application in assessing combined heat, cooling, and power systems.[31] It is still widely accepted for assessing the performance of poly-generation systems,[32–34] and other industrial processes.[35,36] Generally, it utilizes a product-oriented systematic comparison method to calculate the improvement of performance metrics (fuels input, investment cost, etc.) compared to the reference systems. In this work, an exergoeconomic life cycle optimization methodology[37] is developed, which selects the traditional stand-alone systems as the reference systems to obtain the "3-E" indicators in terms of energetic efficiency, economic benefit, and environmental impact, as shown in Figure 3a.

Evaluation approach and indicators

As shown in Figure 3b, supposing a hybrid energy system integrates *f* kinds of feedstocks and *p* kinds of products, such relationship between feedstocks and products can be simplified as an "Input–Output" black box model, in which each feedstock j $(1 \le j \le f)$ will contribute to the production of product i $(1 \le i \le p)$ in a direct or indirect way. But three kinds of inequality can be found: energy level of different feedstocks (e.g., coal and natural gas); energy level of different products (e.g., electricity and liquid fuels), as well as the thermal efficiency of different process pathways. This makes the traditional thermodynamic conversion efficiency unable to assess the overall energetic efficiency and fully reflect the performance improvement. Taking product i $(1 \le i \le p)$ in a hybrid energy system as example, it corresponds to f one-dimensional energy conversion models (1×1). As shown in Figure 2c, to obtain the reference performance benchmark of product i, it is necessary to reduce the dimension and put the performance indicators of these f actual subsystems together. Thus, a virtual $f \times 1$ reference system is constructed with f kinds of feedstock for producing product i, in which the reduced exergetic efficiency factor ($\overline{\eta_i}$), reduced unit exergy investment cost ($\overline{I_i}$), and reduced life cycle waste emissions factor ($\overline{(\mu_i)_k}$) can be deduced as the average performance parameters, as shown in Figure 2d. In this way, we can obtain the evaluation indicators PES, POS, EmA, as well as LCS. Comprehensive details on computing these indicators and average performance parameters are given in SI II.

Systematic analysis and optimization

For a hybrid energy system, the information flows in the "Input–Output" model are highly complex. We can analyze the combination and integration information of process configuration associated with functional units to obtain key integrating factors.[16] Both the RC and OT configurations are classified as a parallel multifeeding structure. Given a feedstock amount of LRC input, biomass and natural gas both affect the flow rate and composition of syngas introduced to Liquid Island. Thus, for the proposed l-CBGTL process, the key integrating factors are biomass/LRC (X_{bc}, kg/kg) and natural gas/LRC (X_{gc}, kg/kg) ratios and the optimum performance can be obtained by adjusting their values. Both the RC and OT configurations are modeled to produce 165×10^6 GGE/year of liquid fuels and 250 MW_x of power. The same basic assumptions for cost and emissions parameters as well as equipment capital cost parameters are used for the

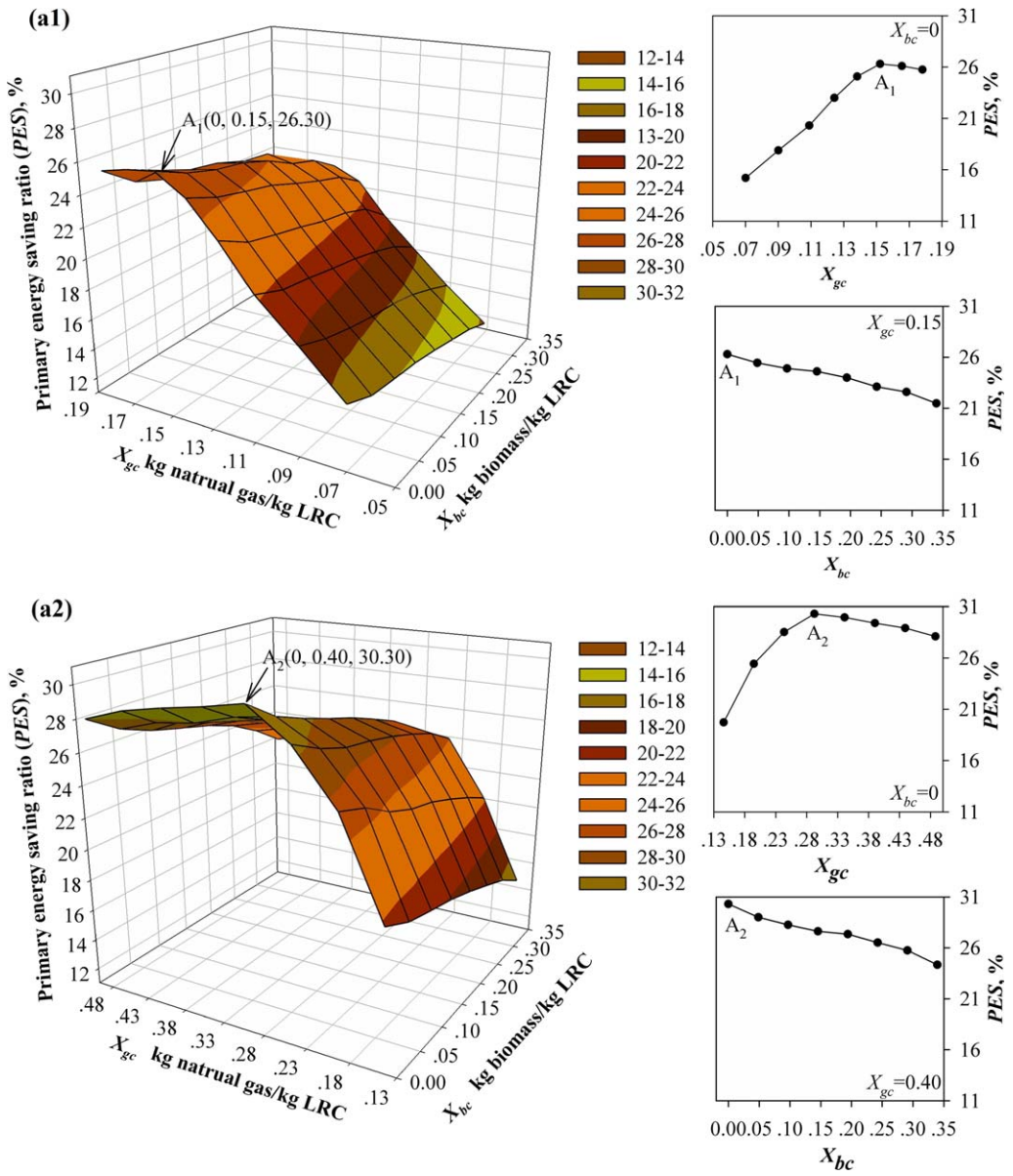

Figure 3. PES, POS, EmA, and LCS indicators of the I-CBGTL process as functions of the key integrating parameters X_{bc} and X_{gc}.

The letters "a," "b," "c," and "d" represent the PES, POS, EmA and LCS indicators, respectively; the numbers "1" and "2" represent RC and OT configurations. [Color figure can be viewed in the online issue, which is available at wileyonlinelibrary.com.]

subreference systems, as listed in Tables S-13 and S-15 of SI II. The results for the optimization of the PES, POS, EmA, and LCS indicators are given in Figure 3. Note that, because of the char/biomass (LHV basis) value is required to be less than 30%,[14,20] the range of varying X_{bc} is 0–0.34 kg/kg. Additionally, to ensure the H_2/CO value falls within the 0.67–2.00 range for LTHT synthesis, the ranges of varying X_{gc} in the RC and OT configurations are 0.15–0.48 kg/kg and 0.07–0.18 kg/kg, respectively.

Figure 3a1, a2 shows the effects of varying the biomass/LRC (X_{bc}) and natural gas/LRC (X_{gc}) parameters on the PES indicator. It can be seen that the PES indicator reaches the highest level for both the RC and OT configurations when the X_{bc} value is 0 (points A_1 and A_2). At these points, the input of biomass is zero and the carbon-rich syngas is totally provided by char gasifying. This happens because an increase of biomass input is harmful for the overall performance of the cogasifier. The input of natural gas has a significant influence on improving the PES indicator at the initial stage. With an increase of X_{gc}, the H_2/CO ratio in raw syngas also experiences an increase which can enhance LTFT synthesis and improve the quality of LTFT syncrude. However, once X_{gc} goes up to a certain extent, the LTFT synthesis rate tends to remain stable and, therefore, the overall exergetic efficiency remains constant, or even drops slightly. Compared to the curve of X_{gc}–PES in the RC configuration, the PES indicator in the OT configuration is slightly more sensitive to the changes in X_{gc}. This is primarily due to the positive impact of H_2-rich syngas which is diluted by the recycle of 97% unreacted gases in the RC configuration. Finally, the calculated highest value of PES for the OT configuration (point A_2) is 30.3%, which is 2.1% bigger than the highest PES value for the RC configuration (point A_1).

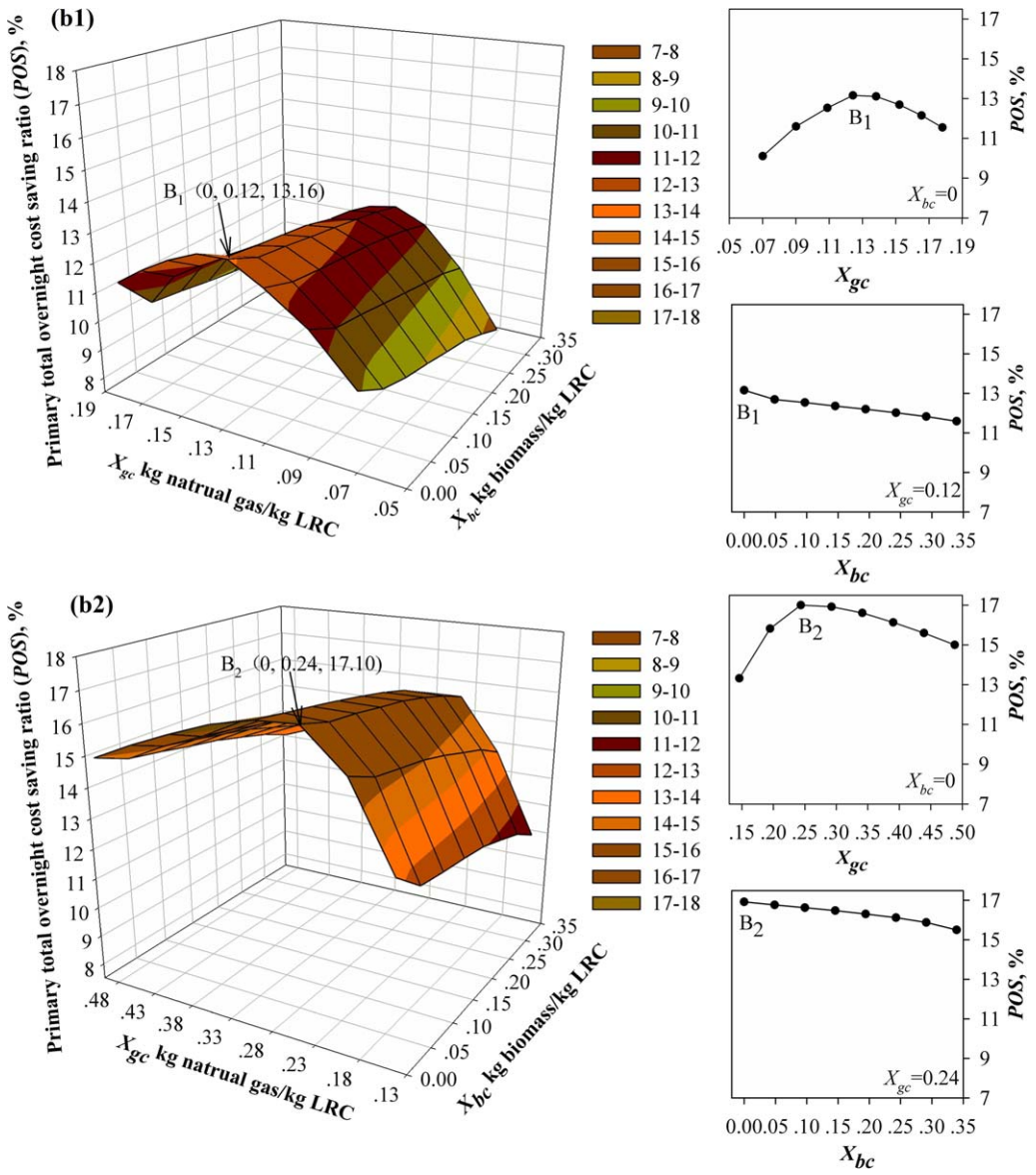

Figure 3. (Continued).

[Color figure can be viewed in the online issue, which is available at wileyonlinelibrary.com.]

Comparing Figures 3b1, b2, a1, a2 indicates that the trends of the POS indicator are similar to those of the PES indicator. As the X_{bc} value is increased from 0 to 0.34, the POS indicator shows a steadily declining trend. This indicates that the addition of biomass results in higher overnight cost for generating per unit exergy output. Higher overnight cost may be attributed to multiple reasons. The energy density of biomass is around 30% lower than that of char, leading to lower cold efficiency, and carbon conversion rate of cogasification. This would incur additional fixed investment of a gasification system to raise the production scale and maintain the same amount of crude syngas output. Increasing the proportion of natural gas in feedstocks helps to improve the conversion rate of feedstocks to liquid fuels production, leading to smaller production scale and investment in upstream gasification section. Besides, improved syncrude quality reduces the installed capital cost of hydro-reactors in the syncrude upgrading unit. As a result, at the initial stage, the input of natural gas leads to savings in the total overnight cost. However, the curves of the POS indicator begin to decline when the values of X_{gc} reach their peaks at B_1 (0, 0.12, 13.16) for the RC configuration and B_2 (0, 0.24, 17.10) for the OT configuration. This may be attributed to a reduction in the growth of LTFT synthesis rate while the fixed investment of expensive ATR reactor in Reform Island continues to increase.

Although the use of biomass as feedstock has an adverse impact on both the energetic efficiency and economic benefit, it can improve the environmental impact indicator EmA significantly, as shown in Figure 3c1, c2. Note that the life cycle GHG emissions of the l-CBGTL process are higher than those of the reference systems when there is no biomass input ($X_{bc} = 0$). From the curves of X_{bc}–EmA, we can see that the RC and OT configurations discharge the same amount of GHG during the life cycle time compared to their reference systems as the respective X_{bc} value rises to 0.08 (point C_1) and 0.10 (point C_2). Hereafter, the EmA indicator continues to increase in a quasi-linear manner with increasing X_{bc}. This result validates that the biomass as a renewable source can play a positive role in reducing life cycle GHG

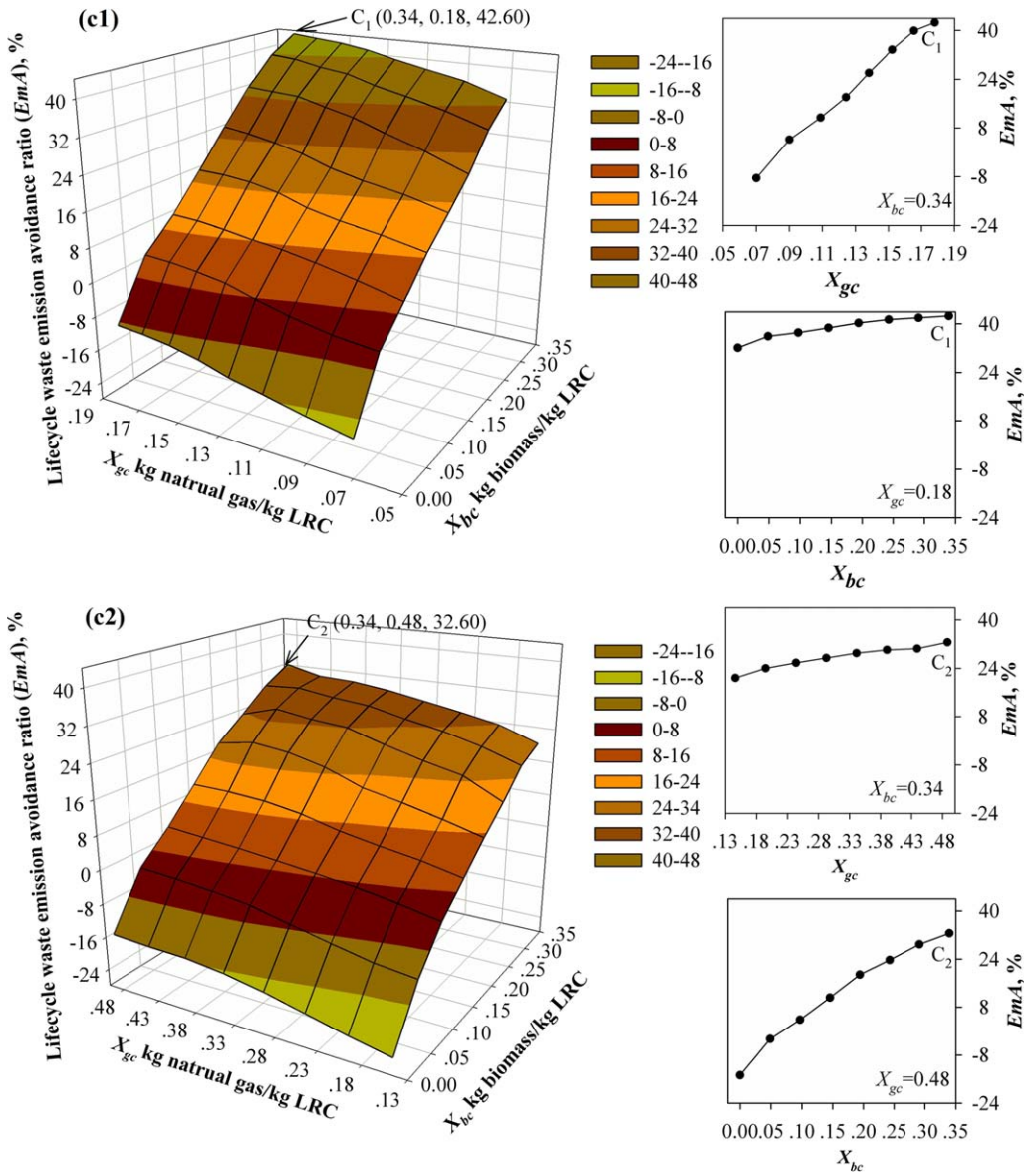

Figure 3. (Continued).

[Color figure can be viewed in the online issue, which is available at wileyonlinelibrary.com.]

emissions. Compared to LRCs, natural gas is a rather clean and low-carbon fuel. For any given X_{bc}, increasing the proportion of natural gas would optimize the hybrid energy mix and decrease the carbon footprint. As shown in this figure, it is found the highest points of the EmA indicator are located at C_1(30.20) and C_2(32.60) when the X_{gc} value rises to the maximum value of 0.34.

Because the LCS indicator is a function of PES, POS, and EmA, it can reflect the overall performance improvement resulting from system integration and process optimization. As shown in Figure 3d1, d2, the X_{gc}–LCS curve of the LCS indicator exhibits a trend similar to that of the PES and POS indicators, which is found to increase and then decrease at point D_1 ($X_{gc} = 0.14$) for the RC configuration and point D_2 ($X_{gc} = 0.24$) for the OT configuration. Moreover, the X_{gc}–LCS curve is found to be rather sensitive to increasing values of X_{gc} instead of X_{bc}. When the X_{gc} value is increased from 0.24 to 0.48, the LCS indicator for the OT configuration is reduced by 17.91%, from 32.28% to 26.50%. From the curves of X_{bc}–LCS in this figure, it can be seen that the LCS indicator increases slowly, giving the highest point at D_1 ($X_{bc} = 0.29$) for the RC configuration and at D_2 ($X_{bc} = 0.24$) for the OT configuration. Both points are located close to the maximum boundary of biomass input ($X_{bc} = 0.34$). As discussed above, the key integration factor X_{bc} enhances the EmA indicator but exerts a negative impact on the PES and POS indicators. Therefore, the D_1 and D_2 points represent the performance trade-off among energetic efficiency, economic benefit, and environmental impact under the given conditions. Note that high carbon tax would further stimulate and expand the share of biomass input in the l-CBGTL process.

Results and Discussion

Optimization results

The previous section gives the results of key integrating parameters for the proposed l-CBGTL process by optimizing energetic efficiency, overnight cost, environmental impact, and levelized cost. Accordingly, we can determine four types

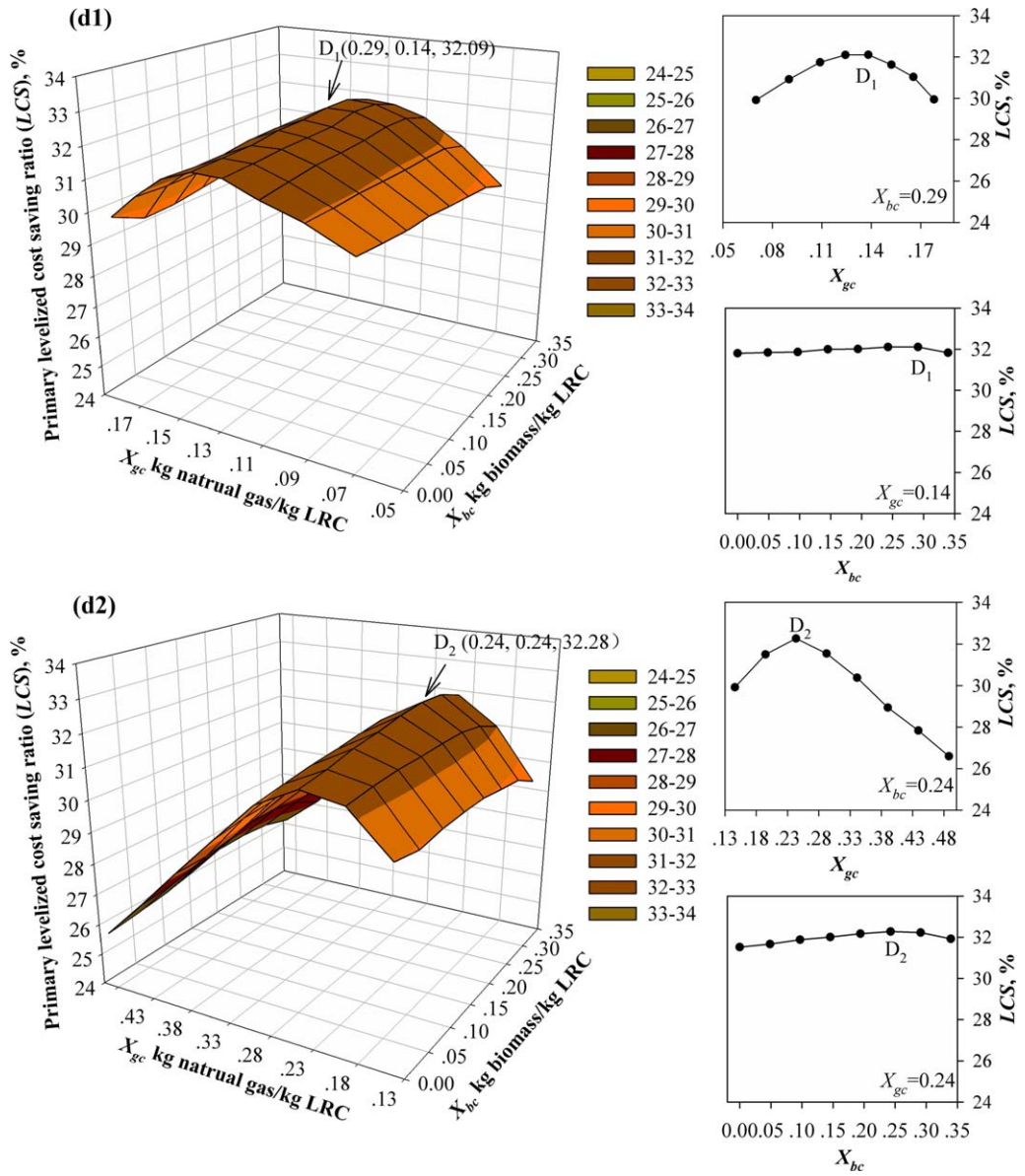

Figure 3. (Continued).

[Color figure can be viewed in the online issue, which is available at wileyonlinelibrary.com.]

of optimal designs: maximum PES design (point $A_{1,2}$), maximum POS design (point $B_{1,2}$), maximum EmA design (point $C_{1,2}$), and maximum LCS design (point $D_{1,2}$), as listed in Table 2. In this table, the levelized cost is converted to a breakeven oil price (BEOP) in \$/GGE, which is considered as a significant indicator of risk mitigation. Thanks to the low delivered cost of LRC (only about half the price of HRC) and high energy conversion efficiency, all these optimal designs produce cheap liquid fuels which are lower than \$2.2/GGE. In particular, given the electricity selling price (\$60/MWh) and carbon price (\$20/ton CO_2-eq), the BEOPs of the RC and OT configurations can be, respectively, reduced to \$1.89/GGE and \$1.87/GGE in the maximum LCS design.

Exergetic, economic, and environmental impact analysis

Figure 4a, b presents the exergy loss distribution for each process unit. For the two configurations, the largest contribution is from the power plant followed by the biomass/char cogasification unit and LRC pyrolysis unit, each accounting for 29–32%, 20–23%, and 11–15% of the total exergy loss. High exergy loss arises in the power plant because the chemical energy of syngas is converted to physical exergy by direct combustion. As shown in these figures, the maximum EmA design gives rise to the highest total exergy loss compared to the other optimal designs, amounting to 699 MW for the RC configuration and 670 MW for the OT configuration. The main reasons are that the highest biomass inputs in both configurations reduce the overall energetic efficiency and increase the irreversibility of the chemical energy conversion. Conversely, the maximum PES design saves the highest amount of primary fuels and causes the least exergy loss, amounting to 606 MW for the RC configuration and 519 MW for the OT configuration. Moreover, for each optimal design the RC configuration consumes higher total exergy inputs compared to the OT configuration, indicating that the OT configuration can lead to higher energy conversion efficiency.

Table 2. Optimization Results for the RC and OT Configurations

		Max. PES Design		Max. POS Design		Max. EmA Design		Max. LCS Design	
		RC	OT	RC	OT	RC	OT	RC	OT
Input	LRC, MW_x	1089	803	1209	821	910	599	1002	801
	As-received, t/day	4882	3599	5420	3680	4080	2687	4495	3593
	Biomass, MW_x	0	0	0	0	262	173	207	198
	As-received, t/day	0	0	0	0	1385	913	1090	1046
	Natural gas, MW_x	470	665	426	681	462	829	393	553
	Feed rate, t/day	743	1053	674	1077	731	1311	622	876
Output	Gasoline, MW_x	147	153	159	158	159	162	147	149
	Diesel, MW_x	540	534	528	529	526	525	540	538
	Liquid fuels, MW_x	687	687	687	687	685	687	687	687
	Liquid fuels, $\times 10^6$ GGE/year	165	165	165	165	164	165	165	165
	Gross power, MW_x	352	338	358	335	350	337	327	325
	Onsite consumption, MW_x	87	76	90	75	100	93	82	75
	Net power, MW_x	265	262	268	260	250	244	245	250
Total overnight cost, $MM		1577	1493	1575	1487	1602	1517	1542	1484
Life cycle GHG emissions, kton/year		1309	1405	1353	1430	680	801	802	897
Total levelized cost, $MM		446	449	446	443	448	467	431	433
Breakeven oil price (BEOP), $/GGE[a]		1.90	1.93	1.89	1.89	1.99	2.13	1.89	1.87

[a]The calculation method of BEOP is reported by Kreutz et al.[11]

The total overnight cost distribution for each process unit is depicted in Figure 5a, b. The biomass and char cogasification unit and power plant are the most expensive units, accounting for 23–27% and 17–20% of the total investment, respectively. Except for the natural gas reforming and hydrogen production unit, most process units in the RC configuration have higher overnight cost than those in the OT configuration for the same optimal design. In the OT configuration, the natural gas reforming and hydrogen production unit has a greater production scale, causing its investment cost to be 1.5 times higher than that in the RC configuration. For the maximum EmA design, the H_2/CO ratio of the syngas introduced to the LTFT reactor needs to be raised to 2.0 in the OT configuration. This raises the overnight cost of the natural gas reforming and hydrogen production unit to the highest value of $305 MM. Further, the maximum EmA design has the highest total overnight cost, amounting to $1617 MM for the RC configuration and $1528 MM for the OT configuration. However, the corresponding numbers for the maximum POS design are only $1569 MM and $1483 MM.

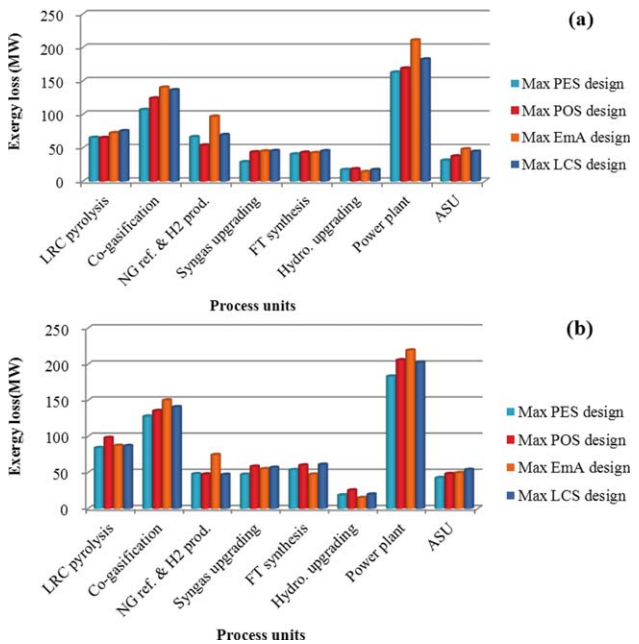

Figure 4. Exergy loss distribution among the optimal designs for each process unit.

(a) RC configuration; (b) OT configuration. [Color figure can be viewed in the online issue, which is available at wileyonlinelibrary.com.]

As shown in Figure 6a, b, different process designs and life cycle stages exhibit different distributions of life cycle GHG emissions. The GHG emissions in the preplant stage and postplant stage together with biomass input determine the total emissions. In the life cycle plant stage, around 90% of process CO_2 is captured and stored, contributing only 3–10% to the total GHG emissions of this stage. Both the maximum PES and POS designs have no biomass input, thus the respective greatest amount of primary fuels saving and overnight cost saving is achieved at the expense of high GHG emissions. Particularly, the maximum POS design reaches its peak of life cycle GHG emissions. Note that in the maximum EmA and LCS designs, although the biomass input takes up only 3–10 LHV% of the total fuels input, the life cycle GHG emissions are reduced by more than 35%. Among the designs, the maximum EmA design can reduce the life cycle GHG emissions of the RC and OT configurations to 674 kton CO_2-eq/year and 789 kton CO_2-eq/year, respectively.

Figure 7a, b shows the primary levelized cost distribution for each optimal design. It includes CO_2 TS&M, GHG emissions tax, fuel costs, O&M costs, and capital charges. At the given carbon price ($20/ton CO_2eq), the sizable contributions are from capital charges (50–56%) followed by fuel costs (17–27%) and O&M costs (15–20%). The main components responsible for the changes in levelized cost are the fuel costs and GHG emissions tax. Compared to the other optimal designs, the fuel costs of the maximum EmA design are increased to the highest proportion (RC: 20%; OT: 27%) because of the highest input ratio of clean but rather expensive feedstocks: biomass and natural gas. On the contrary, the maximum PES design has the lowest fuel costs but pays the highest amount of GHG emissions tax. The maximum

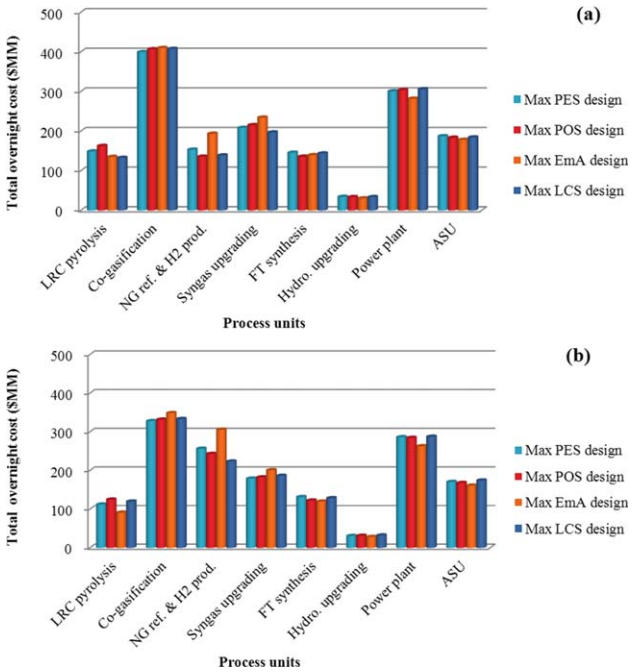

Figure 5. Total overnight cost distribution among the optimal designs for each process unit.

(a) RC configuration; (b) OT configuration. [Color figure can be viewed in the online issue, which is available at wileyonlinelibrary.com.]

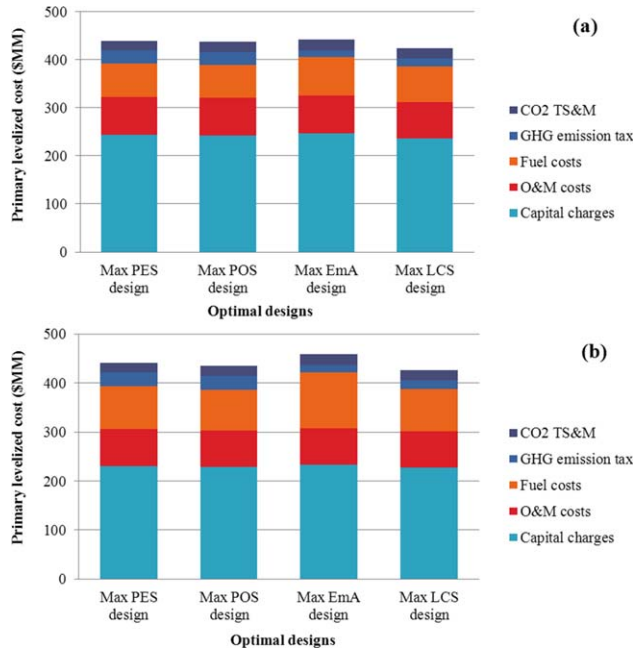

Figure 7. Primary levelized cost distribution for each optimal design.

(a) RC configuration; (b) OT configuration. [Color figure can be viewed in the online issue, which is available at wileyonlinelibrary.com.]

LCS design represents the optimal design of the l-CBGTL process with a unique combination of the fuel costs and GHG emissions tax, which minimizes the primary levelized cost to $421MM for the RC configuration and $425MM for the OT configuration.

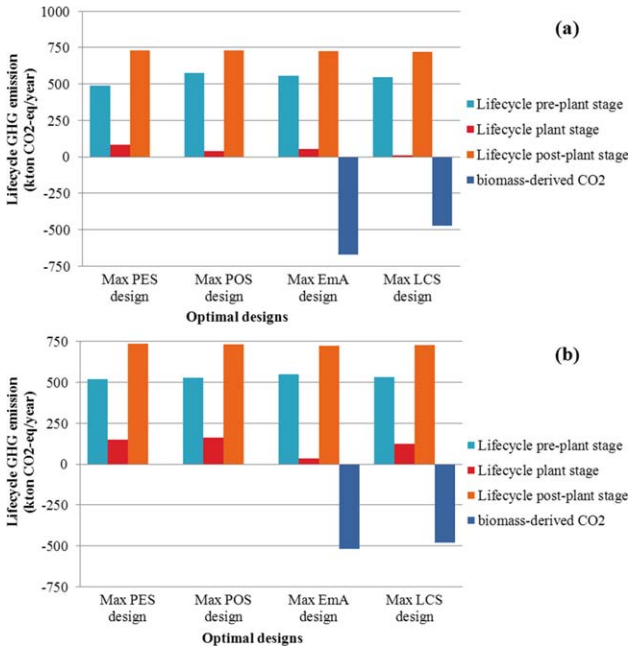

Figure 6. The distribution of life cycle GHG emissions for each optimal design.

(a) RC configuration; (b) OT configuration. [Color figure can be viewed in the online issue, which is available at wileyonlinelibrary.com.]

Finally, it should be noted that there are uncertainties associated with the extent of feedstock conversion and production cost. We briefly analyze the effects of these uncertainties below.

a. In the LRC pyrolysis process, it is assumed that 87% conversion of LRC and 100% recoveries of pyrolysis gas and LRC syncrude are achieved. However, the assumed data may be somewhat optimistic because some industrial cases have reported values that are 4–8% lower than the assumed data,[19] resulting in 4–8%, 8–15%, and 8–15% reductions in the overall yielding rates of char, pyrolysis gas, and LRC syncrude, respectively. Accordingly, the exergy loss of the LRC pyrolysis process would increase from about 55–65 kJ/MJ-LRC to 66–78 kJ/MJ-LRC.

b. Natural gas contributes 51–71% and 62–83% of the total fuel cost in the RC and OT configurations, respectively. Thus, a relatively high delivered price of natural gas (assumed $\$6.35/GJ_{HHV}$ here) brings the BEOP up significantly. Compared to the RC configuration, the OT one achieves a higher energetic efficiency but a lower overnight cost using more than 30 wt % of natural gas as feedstock. It is foreseeable that, with the availability of 20% cheaper unconventional gas (e.g., shale gas, about $\$5/GJ_{HHV}$) as the feedstock, the OT configuration would become more competitive where the BEOP would reduce to about $1.7/GGE.

c. Apart from providing liquid fuels, the l-CBGTL process can also be used for large-scale electricity generation. Electricity is an important product that can be sold to the power grid, generating a profit and reducing the BEOPs of liquid fuels. As indicated in Figure 8, both the increased carbon price and revenue from electricity sales help the l-CBGTL process to mitigate the risk of low oil prices. Under the current carbon price level ($P_{CO_2} < \$40$/ton CO2-eq), the liquid fuels generated from the OT configuration have a minor economic advantage over those from the RC

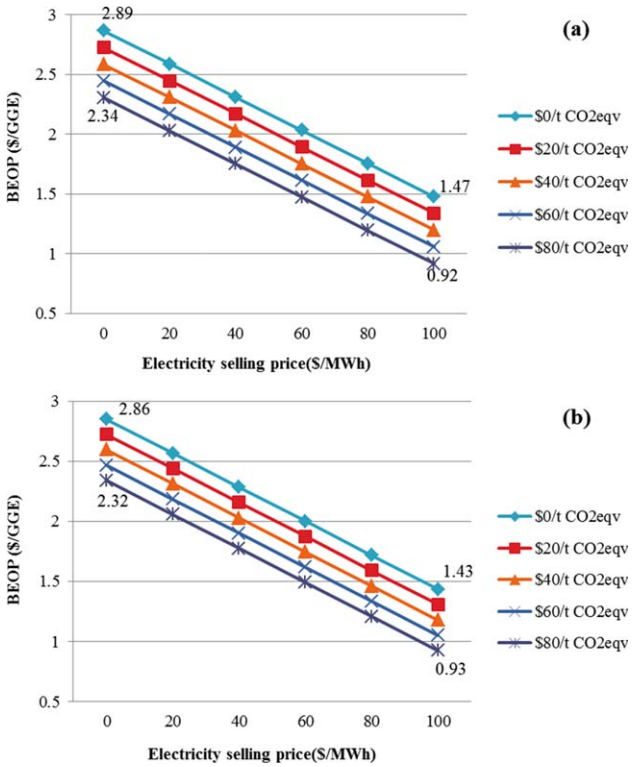

Figure 8. Effects of electricity selling price and carbon price on the BEOP (max. LCS design).

(a) RC configuration; (b) OT configuration. [Color figure can be viewed in the online issue, which is available at wileyonlinelibrary.com.]

configuration. However, if a sufficiently strong carbon mitigation policy is adopted, one might see a reversal of the economic situation.

d. The overnight cost associated with equipment purchase and installation is another source of uncertainty. It is well known that most of the literature costing correlations have at least 10–20% error.[39] This translates to 6–11% error in the capital cost listed in Table 2. However, this uncertainty has a negligible impact on the result of each optimal design. This is because the proposed optimization methodology is based on the relative saving indicator, which makes the errors of overnight cost disappear when the l-CBGTL systems and their reference systems use the same calculation basis.

Comparison with other works

As mentioned in Introduction, several other hybrid feedstocks processes have been conceptually proposed, all of which include at least one step that involves gasification of coal and/or biomass, and/or reforming of natural gas.[8,13,15,20,27] These processes specify syngas as the single intermediate. However, LRCs are not suitable for these processes because of their LHVs. Using an advanced pyrolysis technique, an LRC may first be catalytically converted to useful char, syncrude, and pyrolysis gas without having to deal with problematic impurities. Then, it is possible to cofeed the resulting high heating value char (>28 MJ/kg) with biomass in the Shell-type gasifier. Another unique approach is the corefinery of LTFT and LRC syncrudes to produce on-specification liquids. The approach uses a stoichiometry-based refinery strategy to boost the octane value of gasoline without increasing the aromatic contents.

Mathematical model-based optimization is widely used to determine trade-off designs and optimal conditions.[13,15,20,27] This article proposes a rather special life cycle optimization approach based on an exergoeconomic viewpoint. Although several similar evaluation and optimization approaches have been proposed, they have not been evaluated systematically with simultaneous consideration of life cycle GHG emissions.[32–34] Unlike previous biobjective or global optimization studies,[38,40] the environmental impact objective proposed here, that is, life cycle GHG emissions, is present in terms of the EmA indicator and transformed into cumulative carbon credit in the LCS indicator. Another attractive feature of the proposed approach is that it can clearly disclose the interactions between thermodynamic efficiency, economic benefit, and environmental impact without the need for complex mathematical models.

Concluding Remarks

In this study, a LRC was first used as the main feedstock for a hybrid energy system, and a detailed hybrid LRC/biomass/natural gas process was then proposed for producing liquid fuels and electricity (l-CBGTL). It included two process configurations, namely RC configuration and OT configuration. Based on process simulation, we showed that an exergoeconomy-based life cycle optimization framework can be used to address the optimal design of the sustainable l-CBGTL process, the associated key integrating parameters and production scales. The framework was used to analyze process performance from multiple perspectives of energetic efficiency, economic benefit, and environmental impact. The framework can yield four types of optimal design decisions, namely maximum PES design, maximum POS design, maximum EmA design, and maximum LCS design, among which the maximum LCS design can reflect the overall performance improvement. Given the electricity selling price ($60/MWh) and carbon price ($20/ton CO_2-eq), we can determine four optimal designs which yield competitive BEOPs ranging from $1.87/GGE to $2.13/GGE. In particular, the BEOPs of the RC and OT configurations can be, respectively, reduced to $1.89/GGE and $1.87/GGE in the maximum LCS design.

Acknowledgments

The authors acknowledge financial support from the National High Technology Research and Development Program of China (No. 2011AA05A202) and the National Basic Research Program of China (973 Program: 2012CB720500). This work is partially supported by the Institute for Sustainability and Energy at Northwestern (ISEN).

Literature Cited

1. Energy Information Administration. Annual Energy Outlook 2010. DOI: DOE/EIA-0383 (2010). http://www.eia.gov/oiaf/aeo/pdf/0383(2010).pdf. Accessed on May 5, 2014.
2. Skov ER, England DC, Henneforth CJ, Rinker FG. Syncrude and syncoal production by mild-temperature pyrolysis process of LRC. In: *AIChE Spring Nation Meeting*. Houston, Texas, 2007.
3. Zhang J, Wang Y, Dong L, Gao S, Xu G. Decoupling gasification: approach principle and technology justification. *Energy Fuels*. 2010; 24(12):6223–6232.
4. Sudiro M, Zanella C, Bertucco A, Bressan L, Fontana M. Dual-bed gasification of petcoke: model development and validation. *Energy Fuels*. 2010;24(2):1213–1221.

5. Li F, Zeng L, Velazquez Vargas LG, Yoscovits Z, Fan L. Syngas chemical looping gasification process: bench-scale studies and reactor simulations. *AIChE J*. 2010;56(8):2186–2199.
6. Jaramillo P, Griffin WM, Matthews HS. Comparative analysis of the production costs and life-cycle GHG emissions of FT liquid fuels from coal and natural Gas. *Environ Sci Technol*. 2008;42(20):7559–7565.
7. Van Vliet OPR, Faaij APC, Turkenburg WC. Fischer–Tropsch diesel production in a well-to-wheel perspective: a carbon, energy flow and cost analysis. *Energy Convers Manage*. 2009;50(4):855–876.
8. Cai R, Jin H, Gao L, Hong H. Development of multifunctional energy systems (MESs). *Energy*. 2010;35(11):4375–4382.
9. Floudas CA, Elia JA, Baliban RC. Hybrid and single feedstock energy processes for liquid transportation fuels: a critical review. *Comput Chem Eng*. 2012;41(11):24–51.
10. Neathery J, Gray D, Challman D, Derbyshire F. The pioneer plant concept: co-production of electricity and added-value products from coal. *Fuel*. 1999;78(7):815–823.
11. Kreutz TG, Larson ED, Liu G, Williams RH. Fischer-Tropsch fuels from coal and biomass. In: *25th Annual International Pittsburgh Coal Conference*, 2008. Pittsburgh, PA.
12. Martín M, Grossmann IE. Simultaneous optimization and heat integration for biodiesel production from cooking oil and algae. *Ind Eng Chem Res*. 2012;51(23):7998–8014.
13. Baliban RC, Elia JA, Weekman V, Floudas CA. Process synthesis of hybrid coal, biomass, and natural gas to liquids via Fischer-Tropsch synthesis, ZSM-5 catalytic conversion, methanol synthesis, methanol-to-gasoline, and methanol-to-olefins/distillate technologies. *Comput Chem Eng*. 2012;47:29–56.
14. Meerman J, Ramírez A, Turkenburg W, Faaij A. Performance of simulated flexible integrated gasification polygeneration facilities. Part A: a technical-energetic assessment. *Renewable Sustain Energy Rev*. 2011;15(6):2563–2587.
15. Liu G, Larson ED, Williams RH, Kreutz TG, Guo X. Making Fischer−Tropsch fuels and electricity from coal and biomass: performance and cost analysis. *Energy Fuels*. 2010;25(1):415–437.
16. Jin H, Lin R. *Integrated Energy System of Gas Turbine and Comprehensive Cascade Utilization of Thermal Energy*. Beijing: Science Press, 2008.
17. Liu K. Medium & low temperature pyrolysis system for coal and process for producting upgrading coal, pyrolysis gas with high calorific value and tar or liquefied synthetic oil by using the same. WIPO Patent: 2012/051922 A1, 2012.
18. Tawarmalani M, Sahinidis NV. A polyhedral branch-and-cut approach to global optimization. *Math Program*. 2005;103(2):225–249.
19. Jinsheng G, Dexiang Z. *Coal Liquefaction Technology*. Beijing, China: Chemical Industry Press, 2005.
20. Chen Y, Adams TA, Barton PI. Optimal design and operation of static energy polygeneration systems. *Ind Eng Chem Res*. 2010; 50(9):5099–5113.
21. Field RP, Brasington R. Baseline flowsheet model for IGCC with carbon capture. *Ind Eng Chem Res*. 2011;50(19):11306–11312.
22. Adams TA, Barton PI. High-efficiency power production from coal with carbon capture. *AIChE J*. 2010;56(12):3120–3136.
23. Frey HC, Zhu Y. Improved system integration for integrated gasification combined cycle (IGCC) systems. *Environ Sci Technol*. 2006; 40(5):1693–1699.
24. Panahi M, Rafiee A, Skogestad S, Hillestad M. A natural gas to liquids process model for optimal operation. *Ind Eng Chem Res*. 2011;51(1):425–433.
25. Mantripragada HC, Rubin ES. Performance, cost and emissions of coal-to-liquids (CTLs) plants using low-quality coals under carbon constraints. *Fuel*. 2013;103(0):805–813.
26. Yu G, Xu Y, Hao X, Li Y, Liu G. Process analysis for polygeneration of Fischer–Tropsch liquids and power with CO2 capture based on coal gasification. *Fuel*. 2010;89(5):1070–1076.
27. Baliban RC, Elia JA, Floudas CA. Toward novel hybrid biomass, coal, and natural gas processes for satisfying current transportation fuel demands, 1: process alternatives, gasification modeling, process simulation, and economic analysis. *Ind Eng Chem Res*. 2010;49(16):7343–7370.
28. Bechtel. *Baseline Design/Economics for Advanced Fischer-Tropsch Technology*. Contract No.DE-AC22–91PC90027, U.S. Department of Energy, 1992. Pittsburgh, PA.
29. De Klerk A. Fischer–Tropsch fuels refinery design. *Energy Environ Sci*. 2011;4(4):1177–1205.
30. Guo X, Liu G, Larson ED. High-octane gasoline production by upgrading low-temperature Fischer–Tropsch syncrude. *Ind Eng Chem Res*. 2011;50(16):9743–9747.
31. Havelský V. Energetic efficiency of cogeneration systems for combined heat, cold and power production. *Int J Refrig*. 1999;22(6):479–485.
32. He C, Feng X. Evaluation indicators for energy-chemical systems with multi-feed and multi-product. *Energy*. 2012;43(1):344–354.
33. Lin H, Jin H, Gao L, Han W. Techno-economic evaluation of coal-based polygeneration systems of synthetic fuel and power with CO2 recovery. *Energy Convers Manage*. 2011;52(1):274–283.
34. Lin H, Jin H, Gao L, Han W. Economic analysis of coal-based polygeneration system for methanol and power production. *Energy*. 2010;35(2):858–863.
35. Hasanuzzaman M, Rahim NA, Saidur R, Kazi SN. Energy savings and emissions reductions for rewinding and replacement of industrial motor. *Energy*. 2011;36(1):233–240.
36. Saidur R, Mekhilef S. Energy use, energy savings and emission analysis in the Malaysian rubber producing industries. *Appl Energy*. 2010;87(8):2746–2758.
37. Yue D, You F, Snyder SW. Biomass-to-bioenergy and biofuel supply chain optimization: overview, key issues and challenges. *Comput Chem Eng*. 2014;66:36–56.
38. Martín M, Grossmann IE. Energy optimization of bioethanol production via gasification of switchgrass. *AIChE J*. 2011;57(12):3408–3428.
39. Gong J, You F. Global optimization for sustainable design and synthesis of algae processing network for CO2 mitigation and biofuel production using life cycle optimization. *AIChE J. In press*.
40. Wang B, Gebreslassie BH, You F. Sustainable design and synthesis of hydrocarbon biorefinery via gasification pathway: integrated life cycle assessment and technoeconomic analysis with multiobjective superstructure optimization. *Comput Chem Eng*. 2013;52:55–76.

Manuscript received Nov. 21, 2013, and revision received June 25, 2014.